Sports Medicine (2020) 50:263–282
https://doi.org/10.1007/s40279-019-01210-w

REVIEW ARTICLE

Infrared Thermography in Exercise Physiology: The Dawning of Exercise Radiomics

Barlo Hillen[1] · Daniel Pfirrmann[1] · Markus Nägele[2] · Perikles Simon[1]

Published online: 16 November 2019

Abstract

Infrared thermography (IRT) is a non-invasive tool to measure the body surface radiation temperature (T_{sr}). IRT is an upcoming technology as a result of recent advancements in camera lenses, detector technique and data processing capabilities. The purpose of this review is to determine the potential and applicability of IRT in the context of dynamic measurements in exercise physiology. We searched PubMed and Google Scholar to identify appropriate articles, and conducted six case experiments with a high-resolution IRT camera (640 × 480 pixels) for complementary illustration. Ten articles for endurance exercise, 12 articles for incremental exercise testing and 11 articles for resistance exercise were identified. Specific T_{sr} changes were detected for different exercise types. Close to physical exertion or during prolonged exercise six recent studies described "tree-shaped" or "hyper-thermal" surface radiation pattern (P_{sr}) without further specification. For the first time, we describe the T_{sr} and P_{sr} dynamics and how these may relate to physiological adaptations during exercise and illustrate the differential responsiveness of P_{sr} to resistance or endurance exercise. We discuss how bias related to individual factors, such as skin blood flow, or related to environmental factors could be resolved by innovative technological approaches. We specify why IRT seems to be increasingly capable of differentiating physiological traits relevant for exercise physiologists from various forms of environmental, technical and individual bias. For refined analysis, it will be necessary to develop and implement standardized and accurate pattern recognition technology capable of differentiating exercise modalities to support the evaluation of thermographic data by means of radiomics.

1 Introduction

Infrared thermography (IRT) is a non-invasive and mobile tool to measure and portray changes of the body surface radiation temperature (T_{sr}) in real time. In recent years, IRT is increasingly applied in different scientific fields, due to technological advancements in camera lenses and improvements in the detector technique.

So far, the strength of IRT in the field of medical diagnostics can be attributed to static measurements, e.g. breast cancer, diabetic neuropathy, peripheral vascular disorders [1]. In sports science, IRT measurements are also conducted for sports medical issues, requiring a static application, and exercise physiological questions, requiring dynamic measurements. Static temperature pattern recognition has been applied for the detection of inflammation or injury [2, 3]. A recent review mainly focused on static measurements and highlighted the technical, environmental as well as the internal and external individual factors influencing IRT measurements [4]. The review by Fernandez-Cuevas et al. [4] is a hallmark, since it is particularly elaborate about the multitude of confounders that may hamper a clear readout, delivering valid information on internal individual factors, which are finally relevant for medical diagnostic purposes or for understanding the physiology of thermoregulatory processes. While the assessment of static measurements is more straightforward, and may require less sophisticated settings and technical equipment, their drawback is that they will not provide enough information to allow a discrimination

Electronic supplementary material The online version of this article (https://doi.org/10.1007/s40279-019-01210-w) contains supplementary material, which is available to authorized users.

✉ Perikles Simon
simonpe@uni-mainz.de

[1] Department of Sports Medicine, Rehabilitation and Disease Prevention, Faculty of Social Science, Media and Sport, Johannes Gutenberg University Mainz, Albert Schweitzer Straße 22, 55128 Mainz, Germany

[2] OptoPrecision GmbH, Auf der Höhe 15, 28357 Bremen, Germany

Key Points

Recent studies reported a progressively developing surface radiation pattern (P_{sr}) during exercise.

Surface radiation temperature (T_{sr}) and pattern (P_{sr}) changes observed by IRT can be related to specific acute skin blood flow adaptations for each exercise type.

In analogy to typical radiomics approaches, time series analysis will be required to enable valid prediction of physiological traits.

between the relative importance and the individual impact of environmental, individual and technical confounders for the measurement of relevant exercise physiological readouts. This is where dynamic measurements come into play. Dynamic measurements could principally provide enough data points to subtract the background noise caused by influential factors from the dynamic temperature patterns, which ideally can be correlated with physiological readouts. For example, particularly during prolonged or intensive exercise, the imminent and significant increase of core temperature has been implicated as one of the most limiting factors for exercise performance [5]. The measurable surface radiation temperature could possibly deliver information about the core temperature or the individual thermoregulatory capacity, but this hypothesis is yet rather vague.

During past decade, the development in infrared camera systems made significant progress in terms of sensitivity (temperature resolution: typ. 35 mK), measurement speed (frames/second: up to 100 Hz) and especially in the spatial resolution (number of pixels: typ. 640 × 480). Moreover, due to the increasing widespread use of those systems, the sales figures rose and the price per unit dropped considerably. All these factors are highly beneficial for its application in sports science. The purpose of this review is to determine the potential and applicability of IRT in the context of dynamic measurements in exercise physiology.

In the following, we shall at first summarize the studies that applied IRT for measurements in constant load endurance exercise (EE—is here defined as running, cycling or rowing, that lasts longer than 10 min, with a constant or incremental increasing intensity), incremental exercise testing (XT—is here defined as running, cycling or rowing of an incremental increasing intensity protocol until exhaustion), as well as resistance exercise (RE—is here defined as a load, which lasts less than 10 min and follows a typical resistance exercise protocol), and compare these findings with illustrations of own case experiments, carried out with a high resolution IRT camera (Sects. 2, 3, 4; Figs. 1, 2, 3, 4). We shall elucidate the potential of IRT to generate new insights into human exercise physiology (Sect. 5; Fig. 5). We discuss significant influential factors for dynamic measurements in Sect. 6 (Fig. 6). Finally, we briefly list the required possibilities to enhance the analyses of thermograms according to innovative data processing out of digital pictures as applied in radiomics [6] (Sect. 7).

To identify appropriate articles for this narrative review, the search terms (((((“Infrared thermography”[Title/Abstract]) OR “Infrared thermal imaging”[Title/Abstract]) OR “thermal imaging”[Title/Abstract]) OR “thermography”[Title/Abstract]) AND “exercise”[Title/Abstract]) AND (“1992”[Date - Publication] : “2018”[Date - Publication]) were applied in PubMed and Google Scholar. Additional articles were searched for in the reference lists of the included articles. All studies that examined human subjects during exercises, including EE, RE and XT with an IRT camera, were appropriate. Furthermore, only peer-reviewed articles in English were included. The methods of our own case experiments are explained in the figure legends (Figs. 1, 2, 3, 4).

2 IRT in Constant Load Endurance Exercise

From the last 26 years (1992–2018), only ten articles were identified which can be related to the observation of IRT in constant load endurance exercise (EE) (Table 1) [7–16]. The results are limited by a low total number of subjects ($n = 99$), different camera systems, outcome parameters, ROI, various exercise intensities, and durations of EE. The recording procedures and thermogram analyses also differed between the examinations. For instance, the primary outcome for the measurements is the average temperature, consisting of a combination of different regions of interest (ROI). The ROI were mostly the upper body, back and front, and the lower and upper extremities, also back and front surface. Priego Quesada et al. [11] examined the muscle-related ROI over the entire body, and Zontak et al. [15] observed only the surface temperature of the hands. Most research groups evaluated the outcome parameter “skin temperature” (T_{sk}). Furthermore, some studies evaluated only one ROI, which impedes a comparison of inactive and active limbs. Tanda [7] calculated the arithmetic mean of 18 different ROI and also found a difference in the temperature change between the upper limbs and the thigh. Balci et al. [8] only analyzed chest and back as ROI during cycling. Priego Quesada et al. [11] was the only research group that compared 17 ROI with each other during cycling. They observed a decrease in temperature for trunk and tibialis anterior, but observed an increase for anterior thigh and knee. The core temperature was only measured in two studies [8, 11]. In Balci et al. [8], the core temperature (T_{core}) was measured via an ingestible telemetric temperature sensor. T_{core} increased

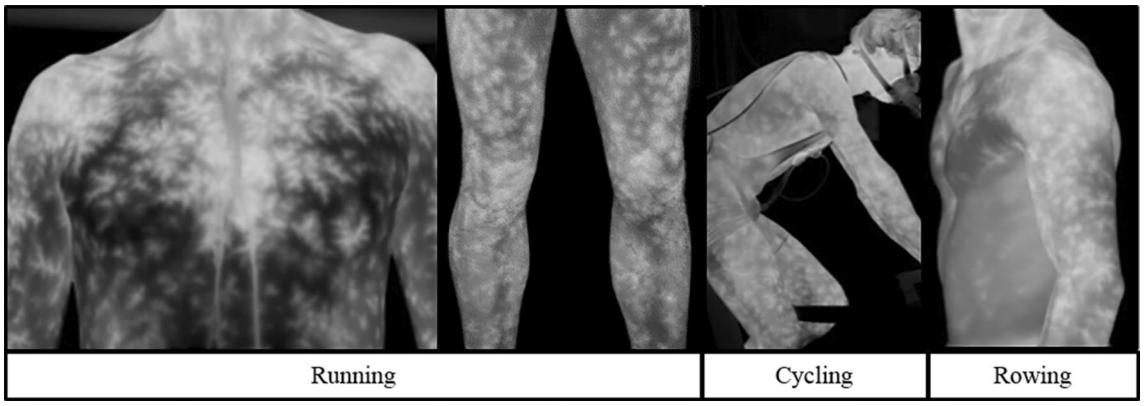

Fig. 1 The surface radiation pattern (P_{sr}) detected immediately after different types of stepwise progressive endurance exercises close to the point of voluntary exhaustion. The first subject was running, the second subject was cycling, and the third subject was rowing. All exercise sessions lasted for about 20 min at normal ambient temperature (20–24 °C). The observed patterns and temperature differences developed gradually with the progressive protocols in all three athletes. For the cyclist, this information is shown in Fig. 2 in more detail. A video of the cycling exercise is presented as supplemental material (S1)

gradually throughout the exercises (submaximal exercise 36.8 to > 37.8 °C; exercise test 36.8 to > 38 °C). In Priego Quesada et al. [11], the core temperature was measured via a core body thermometer enclosed in an ingestible pill. Core temperature for a 45 min constant cycling test at 50% peak power output (increase of 0.8 °C) was 0.2–0.3 °C higher than at 35% (increase of 0.5 °C).

Despite the high variability in characteristics of studies, some common findings can be derived. During continuous EE, the T_{sk} of different ROI decreases immediately after the beginning of exercise. Tanda [7] observed a total T_{sk} decrease of about − 1.4 °C, but a higher decrease in the upper limbs (− 2.0 °C). Other authors [11, 16] reported a positive correlation between load and the decrease of T_{sk} at the initial phase of EE. Immediately after termination of the exercise, researchers observed that the T_{sk} increases again, up to the resting T_{sk} or above [7, 9, 12, 14]. Korman et al. [10] detected a plateau or stabilization of T_{sk} after an initial decline, whereas the majority of authors described a slow increase of T_{sk} following a constant load [7–9, 12, 15]. Thereby, Korman et al. [10] applied a camera system with a high resolution of 640 × 480 pixels, but the remaining investigators used cameras with a lower resolutions of ≤ 320 × 240 pixels. Interestingly, Tanda [7, 12] observed *"hyperthermal spots"*. For the same or at least a similar phenomenon, Balci et al. [8] coined the term *"thermal kinetic pattern"*, which was reported to occur close to the end of EE, in combination with a slight rise of the T_{sk}.

The authors' own investigations, concerning IRT measurements during EE, with a high-resolution IRT camera (IR-TCM 640 × 480 pixels, 7.5–14 µm spectral range, 25 p/s), confirm the findings of the literature and encourage the focus of research on *"hyperthermal spots"* [7] or *"thermal kinetic pattern"* [8]. Figure 1 shows that a mixture of "cold", expressed as dark pixels, and "hot", expressed as light pixels occurs nearly identically during different EEs such as running, rowing, or cycling. Instead of *"hyperthermal spots"*, the light pixels appear more like subcutaneous vascular trees. This surface radiation pattern (P_{sr}) was detected over the entire body surface, especially the upper frontal body, and the extremities. This is the first time that the fine structure of P_{sr} has been illustrated, which could not be detected by cameras with a lower resolution (s. video supplemental material (00:07:50–00:07:55) S1).

Conclusively, it can be summarized, that IRT measurement in EE detects an initial decrease of T_{sk} in different ROI, followed by a plateau phase or an increase of T_{sk} again up to the initial T_{sk} level or above, until the end of the exercise. A further increase of T_{sk} appears immediately after the end of the exercise. This increase of T_{sk} can be linked to the developing P_{sr} which could be revealed during different types of EE over the entire body (Fig. 1).

3 IRT in Incremental Exercise Testing

In the field of incremental exercise testing (XT), IRT has also been increasingly applied throughout the last 10 years (2009–2018). Twelve articles investigated whether there is a significant relationship between physiological parameters (e.g. heart rate (HR), maximum oxygen uptake (VO_{2max}), lactate), and a change of T_{sk} during an incremental exercise test on the ergometer (8/12) or treadmill (4/12) (Table 2) [7, 8, 17–26]. Of these, two articles were already included in the EE section (Sect. 2), since these studies compared both types of exercise [8, 12]. 213 healthy participants were observed with IRT in XT. Similar to EE, an IRT camera resolution of 320 × 240 pixels or lower was applied. In

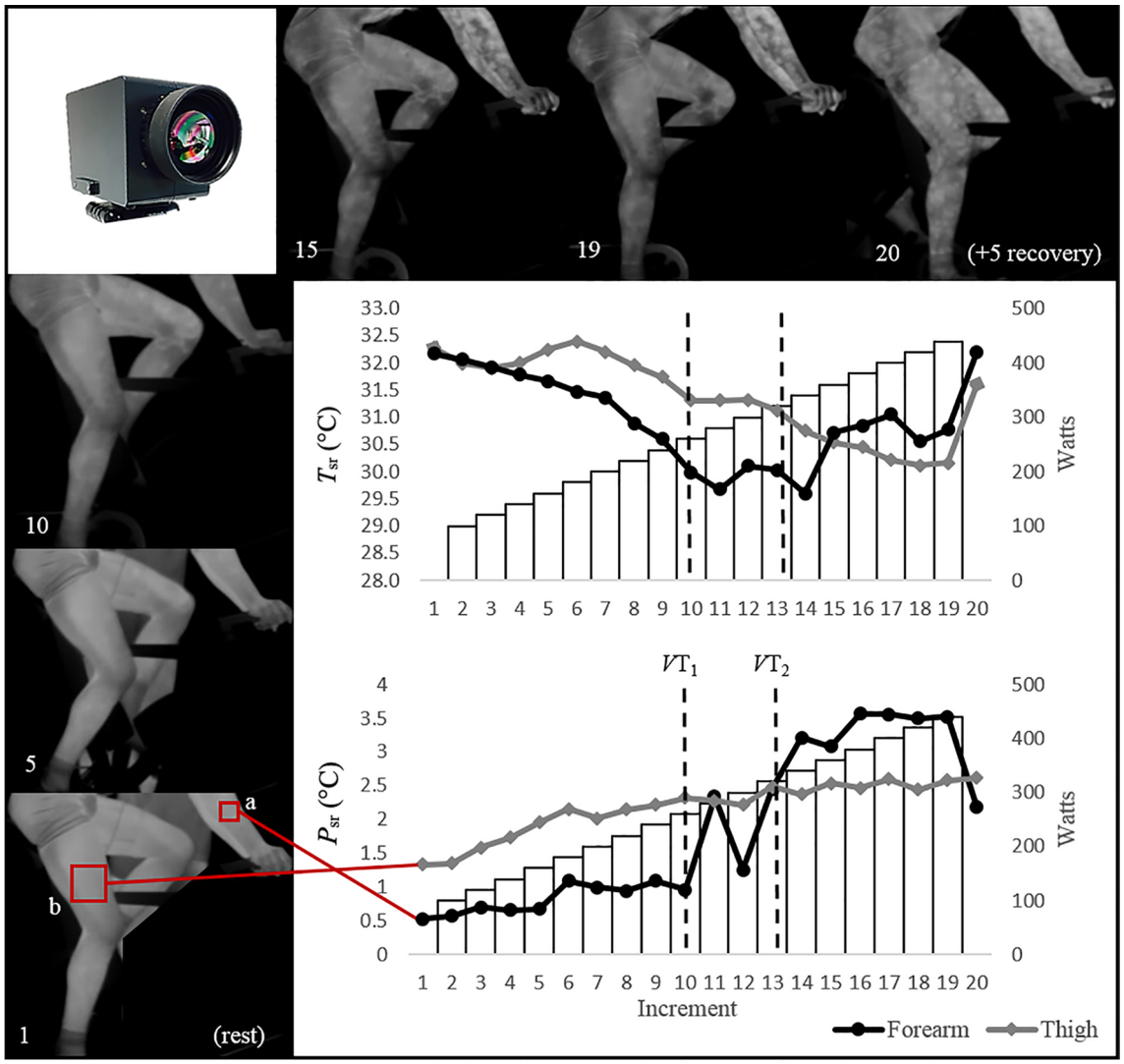

their examinations, researchers mostly focused on the lower extremities (6/12). Four research groups [8, 24–26] were interested in T changes of the anterior and posterior upper body, one [23] concentrated on the forehead and one [7] on T of the entire body.

Similar to EE, a rapid increase of T_{sk} has been detected after the offset of exercise [7, 18, 19, 24]. In contrast to EE, a progressive decrease of T_{sk}, until the point of exhaustion was reported [7, 8, 17–20, 22, 24]. Thereby, research groups observed the magnitude of T_{sk} reduction differently. Tanda [7] reported − 1.4 to − 2 °C, Ludwig et al. [19] − 0.6 to − 1.6 °C, Duc et al. [20] − 2.6 °C and Merla et al. [24] − 3 to − 5 °C. Most of the authors reported no increase of T_{sk} during the XT. Duc et al. [20] detected a significant correlation between HR ($r = -0.8$), O_2 uptake ($r = -0.7$) and T_{sr} ($p < 0.001$). Although, there is almost no reported increase of T_{sk} during XT, *"hyperthermal spots"*, or *"hot spotted pattern"* appeared at the last increments or towards the end of XT [7, 8, 19, 20, 22, 24]. Priego Quesada et al. [18] reported that the T_{sk} response to XT is more pronounced in trained rather than in non-trained subjects. Akimov and Son'kin [23] reported an increase in T_{sk} for endurance athletes and a decrease for untrained persons, until exhaustion in this context. This research group observed a correlation of the 4 mmol lactate threshold with the beginning of the T_{sk} increase in endurance athletes. Arfaoui et al. [22] illustrated that there is a detectable, significant difference of the T_{sk} change between 150 and 200 Watts. The literature shows considerable differences concerning the results of temperature changes during XT with only a few important hints for correlations with physiological parameters.

Observations from our case experiments support and clarify the various findings in the literature. The methods and descriptive results of the authors' case experiment in incremental exercise testing are described and illustrated in Fig. 2. The main observations are that the thigh and the forearm T_{sr} decreased from the beginning to the end of the XT. The P_{sr} appeared during XT and both T_{sr} and P_{sr} parameters

◂**Fig. 2** Forearm and thigh T_{sr} (°C) and P_{sr} (°C) of an endurance athlete during an incremental exercise test on a cycle ergometer (Test protocol: 100 W/20 W/1 min); *VT*1 = ventilatory threshold 1; *VT*2 = ventilatory threshold 2; a = ROI: forearm; b = ROI: thigh. P_{sr} = *10% darkest pixels—10% lightest pixels within the ROI.* This experiment was carried out to verify the results of the state of the art with a high-resolution infrared camera. The T_{sr} and P_{sr} of the forearm and thigh were analyzed as primary parameters. For the calculation of P_{sr}, the difference between 10% of the darkest and 10% of the lightest pixels within the ROI was calculated. HR, VO_2 uptake and lactate were also measured. IRT was applied for the observation of a 24-aged, endurance athlete during an incremental cycling XT. The XT started at 100 Watts and increased 20 Watts each minute, until subjective exhaustion. The IRT camera (640 × 480 pixels) was placed beside the athlete, with a distance of 3 m, to achieve the focus on the lateral forearm and the legs. The ambient temperature was 22 °C. The camera took 25 thermograms per second. The recorded pictures were selected immediately before, after each increment, and 5 min after the XT, considering strict criteria, as followed. An appropriate thermogram is characterized by the highest knee ankle and a sharp thermogram resolution. The ROI were captured manually with a square-shaped box, which did not extend beyond the edge of the extremities. The box was placed in the middle of the right forearm and the right thigh. The athlete completed 18 increments (18 min = 440 Watts). Therefore, a total of 20 thermograms were analyzed. At rest, there is an overall homogeneous T_{sr}. A low variance of light and dark pixels in the measuring box and no P_{sr} were observed. During the XT, different T_{sr} and P_{sr} progressions between the forearm and the thigh appeared. The thigh T_{sr} decreased about 2.1 °C (32.3–30.2 °C) from the beginning to the end of the XT. This reduction was almost continuous and decreased similarly with increasing load. Nevertheless, there was a slight thigh T_{sr} increase of 0.5 °C from stage 3–6 and a plateau phase at stage 10–12 (31.3 °C). Interestingly, this plateau phase was exactly between the ventilatory threshold 1 (*VT*1) and the ventilatory threshold 2 (*VT*2). Meanwhile, the thigh T_{sr} decreased by 1 °C up to *VT*1 (32.3–31.3 °C) and by about one further degree after *VT*2 (31.1–30.1 °C). The forearm T_{sr}, on the other hand, developed differently during the XT. First, the forearm T_{sr} dropped continuously over the first 7 stages by 0.9 °C (32.2–31.3 °C) and then even steeper from stage 7–11 by further 1.6 °C (31.3–29.7 °C). Within the aerobic–anaerobic transition (*VT*1–*VT*2), forearm T_{sr} rose again by 0.4 °C (29.7–30.1 °C); (stage 11–12) and then dropped again by 0.5–29.6 °C until 1 stage after *VT*2 (14). Afterwards, the forearm T_{sr} increased again by 1.2 °C (30.8 °C) up to the maximum load (19) of the athlete, as can be seen in the figure. The P_{sr} appeared during the test and developed differently between the thigh and the forearm. The thigh P_{sr} increased slowly and consistently from 1.3 to 2.6 °C throughout the test. In contrast to thigh P_{sr}, the forearm P_{sr} seems to be more pronounced. Up to *VT*1, the forearm P_{sr} initially increased only slightly (stage 1–10). After *VT*1, however, the forearm P_{sr} increased strongly (1.3 °C), decreased from stage 11–12 (2.3–1.3 °C) and then increased again strongly by 2.3 °C up to stage 16. Overall, the forearm P_{sr} increased from 1.3 to 3.6 °C until exhaustion. After a recovery period of 5 min (stage 20), thigh T_{sr} rose again but remained 0.6 °C below the initial level. Forearm T_{sr}, on the other hand, rose again to the initial level of 32.2 °C. The thigh ΔP_{sr} remained constant but appeared considerably more transparent. The forearm P_{sr} decreased by 1.3 °C and was no longer as sharp as in the previous stages. The HR increased from 56 to 188 beats per minute, the oxygen intake increased from 5.5 to 65.5 ml/min/kg and the lactate concentration increased from 1.4 to 6.82 mmol/l. Five min after recovery the HR was 114 and the lactate concentration was 8.26 mmol/l. A video of the cycling exercise is presented as supplemental material (S1)

developed differently between the thigh and the forearm. Whereas the thigh P_{sr} increased slowly and consistently, the increase in forearm P_{sr} was more pronounced throughout the test (s. video supplemental material (S1)).

The thermograms, as presented in Figs. 1 and 2, are capable of resolving some contradictory findings in the literature. An average T_{sr} is potentially confounded by the presence of P_{sr}, which has so far only been observed by six other research groups [7, 8, 19, 20, 22, 24] to date with little depth of field. The analyses of only single-point measurements to pre- and post-test points is also insufficient for interpreting and transferring the results to physiological changes, due to a non-linear course of T_{sr} and P_{sr} (Fig. 2). As already detected by Priego Quesada et al. [27], a different ROI leads to at least a different T_{sk}. We are the first to describe that P_{sr} is ROI dependent, at least if different extremities are studied (Fig. 2). Different loads during EE and XT can principally be differentiated by IRT [8, 12]. Additionally, it can be claimed that there is a relation between the T_{sr}/P_{sr} changes and the acute neural, cardiovascular and thermoregulatory adaptations (Sect. 5). The dominant detected P_{sr} in EE and XT is the surface radiation of the individual perforasome (PP_{sr}) (Sect. 5).

4 IRT in Resistance Exercise

In recent times, there has also been a considerable rise in the application of IRT in resistance exercise (RE). Eleven articles, published between 2007 and 2018, are summarized in Table 3 [28–38]. Overall, 209 heterogeneous participants were observed. The studies also varied in technical and methodological conditions and an IRT camera with a resolution of 320 × 240 pixel (5/11) was usually applied [29, 31–33, 35]. The other authors did not report on the camera resolution [30, 36–38] or used a lower resolution (160 × 120) [34]. The comparison of thermograms between 2007 and 2018 revealed a strong difference in the image quality and different time points were chosen for the thermogram selection. This may at least partially explain controversial findings between studies. For instance, most research groups reported an increased "skin temperature" (T_{sk}) related to the stressed muscles [28–30, 33, 35, 36, 38], whereas three others reported a decrease [31, 32, 34]. In contrast, Ferreira et al. [37] did not detect any change in the T_{sk} during RE. Overall, the T_{sk} changed by about 0–1.8 °C in RE, but it is particularly controversial whether T_{sk} increases or decreases in the course of a RE. Even if mostly the same ROI have been examined, the findings are incomparable due to different exercise protocols, subjects and measuring time points. The most researched ROI are the biceps brachii and the thigh surface areas. Five research groups examined the

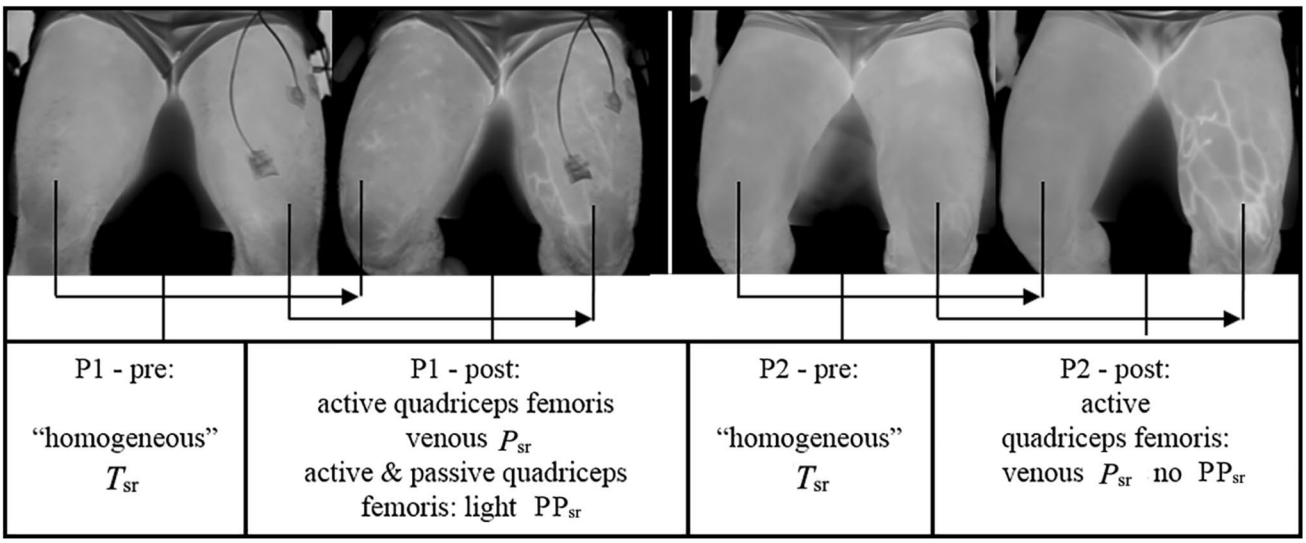

Fig. 3 Venous P_{sr} of two subjects after an all-out knee extension RE. Two healthy men performed one set of all out, unilateral knee extension, with the left leg, against resistance of 17.5 kg, which was equivalent to about 15–20% of their one repetition maximum. P1 (age 25) can be characterized as a mixed active and P2 (age 45) as a former running athlete. The ROI was the anterior surface of the thighs. A camera distance of 1 m was applied to obtain the highest possible resolution. The ambient temperature was approximately 22 °C. P1 fulfilled 70 repetitions in 2:30 min. P2 accomplished 90 repetitions in 3:00 min. Videos of the knee extension case experiment are presented as supplemental material. Videos of the strength exercise P1 and P2 are presented as supplemental material (S2 and S3)

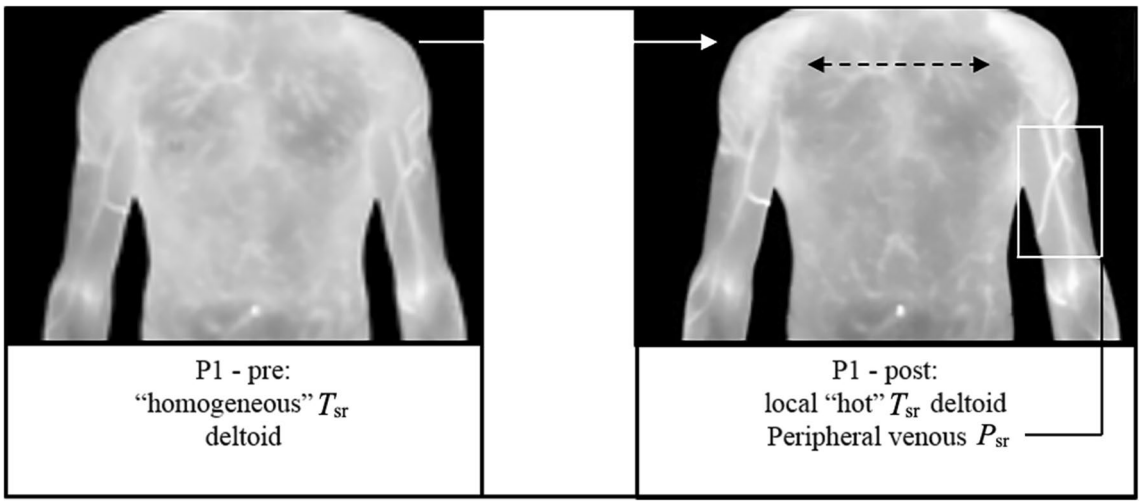

Fig. 4 T_{sr} of the deltoideus after three sets of barbell shoulder press with 70% of the 1RM. Venous P_{sr} over the peripheral biceps area. The subject was a 25-year-old, male, left-handed and mixed active. Barbell shoulder press was performed for three sets of ten repetitions (70% of the 1 repetition maximum), with 1-min rest between each set. The ROI was the anterior surface of the upper body, especially the surface of the shoulders. A camera distance of 3 m was determined. The ambient temperature was about 21 °C. The subject needed about 9 min to fulfill the target of sets and repetitions

thigh [29–32, 37] and four the biceps brachii [28, 31, 33, 36]. Whereas Weigert et al. [28] detected a T_{sk} increase of 1.8 °C during bicep curls, Neves et al. [33] detected a T_{sk} decrease during unilateral biceps curls. Al Nakhli et al. [36], in turn, reported an increase of biceps brachii T_{sk} of 1.1 °C, but this increase was detected at 24 h post RE, without reporting on measurements of T_{sk} immediately after exercise. For the examination of the thigh T_{sk}, three investigators [29, 30, 32] detected a T_{sk} increase and one [37] measured no T_{sk} difference pre- and post-exercise.

Despite the heterogeneous methodology, studies reported concordant findings concerning the thermal changes in relation to different performance levels, contralateral effects and the execution time of the exercises. Sillero-Quintana et al. [30]

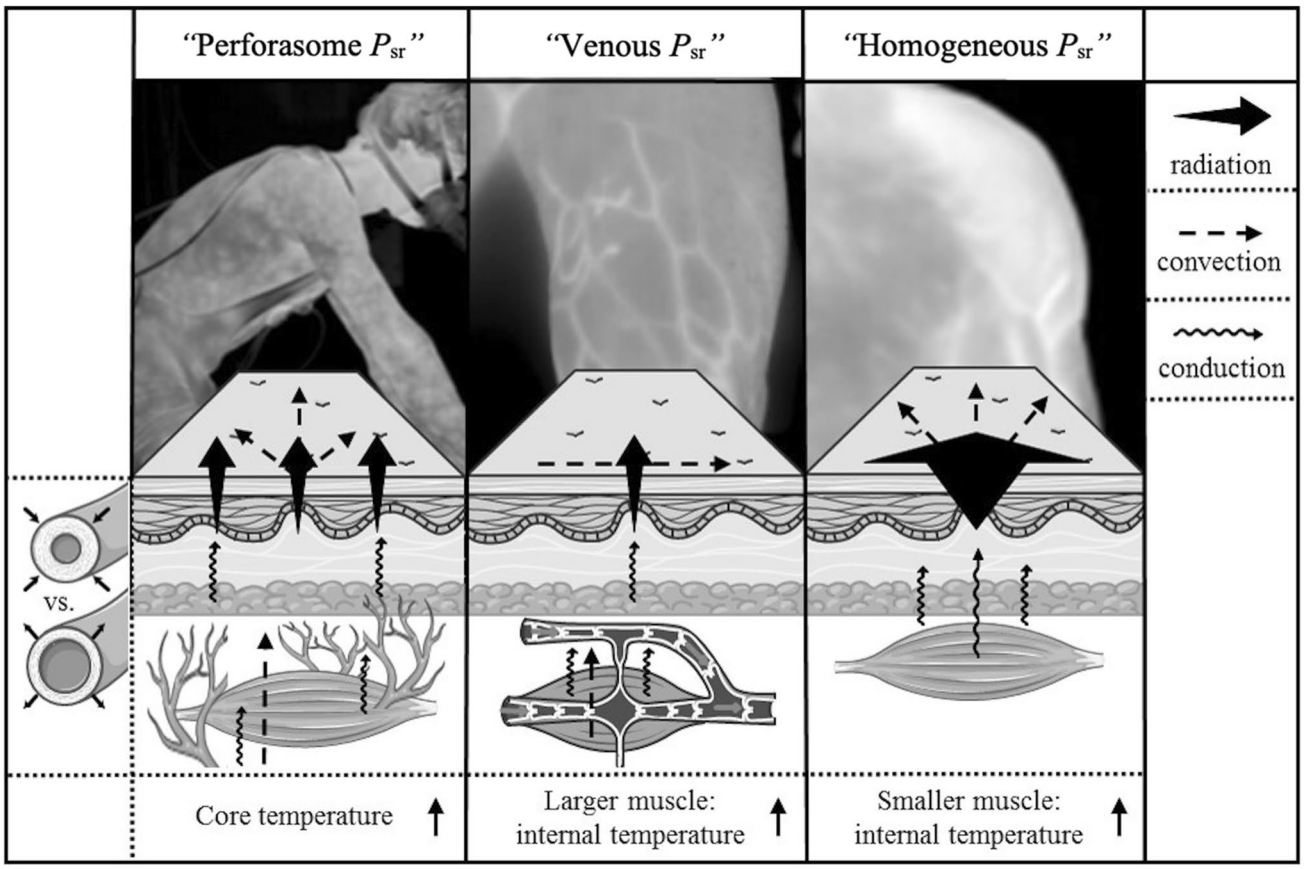

Fig. 5 Three exercise induced surface radiation pattern types. Graphical elements from Servier Medical Art (licensed under a Creative Common Attribution 3.0 Generic License. http://smart.servier.com/) were modified in Fig. 5

discovered a difference between "low-" and "high-trained" individuals. This observation is also confirmed by Formenti [35]. As a result, the T_{sk} increased by an average of 1 °C for the "trained" collective, whereas a lower increase of 0.4 °C could be observed in the "untrained" group. In the trained group, the T increased more quickly than in the untrained group. In the same study, only a difference in T_{sk} between older and younger subjects was observed before RE [37]. In two studies [28, 31], the investigators focused on the relationship between the intensity of exercise and the extent of change in T_{sk}. Accordingly, a difference in the intensity of RE showed no significant difference in the change of T_{sk} during RE. Formenti et al. [32] compared the execution time of the movement, which produced a significant effect. Interestingly, Formenti et al. [32, 35] analyzed the different parameter "T_{max}", which is the automated selection of the warmest pixels within the ROI. They found that while ΔT_{sk} remained unchanged with different execution times, T_{max} decreased more slowly with a more extended exercise execution [32]. T_{sk} changes did not differ between the active and passive extremities in unilateral RE [30, 36].

In contrast to EE and XT, no research group reported on a surface radiation pattern. Contrastingly, two complementary case experiments by the authors revealed specific T_{sr} and P_{sr} variations due to different cutaneous blood flow adjustments during RE.

In case experiment one, two subjects (P1, P2) performed a one-legged knee extension (Fig. 3). At rest, there was a nearly homogeneous T_{sr} on each leg and between the active left and the passive right leg, for both subjects. During the RE, P1's T_{sr} changed differently from the T_{sr} of P2. At the end of the set, there was a clear venous P_{sr} on the left, active side. This venous P_{sr} increased slowly throughout the test procedure. Simultaneously, a light PP_{sr} manifested on the left, active and right, passive thigh. Likewise, the venous P_{sr} appeared on the active thigh of P2, but with higher radiation intensity than on P1's thigh. Conversely, no PP_{sr} was detectable for P2 (s. videos supplemental material S2 and S3).

In case experiment two, a subject performed a barbell shoulder press (Fig. 4). Here, RE of the smaller upper body muscle mass (deltoideus) led to a high, homogeneous local T_{sr} of the shoulders. In contrast to case experiment one, venous P_{sr} did not appear above the stressed body parts, but in the adjacent peripheral areas.

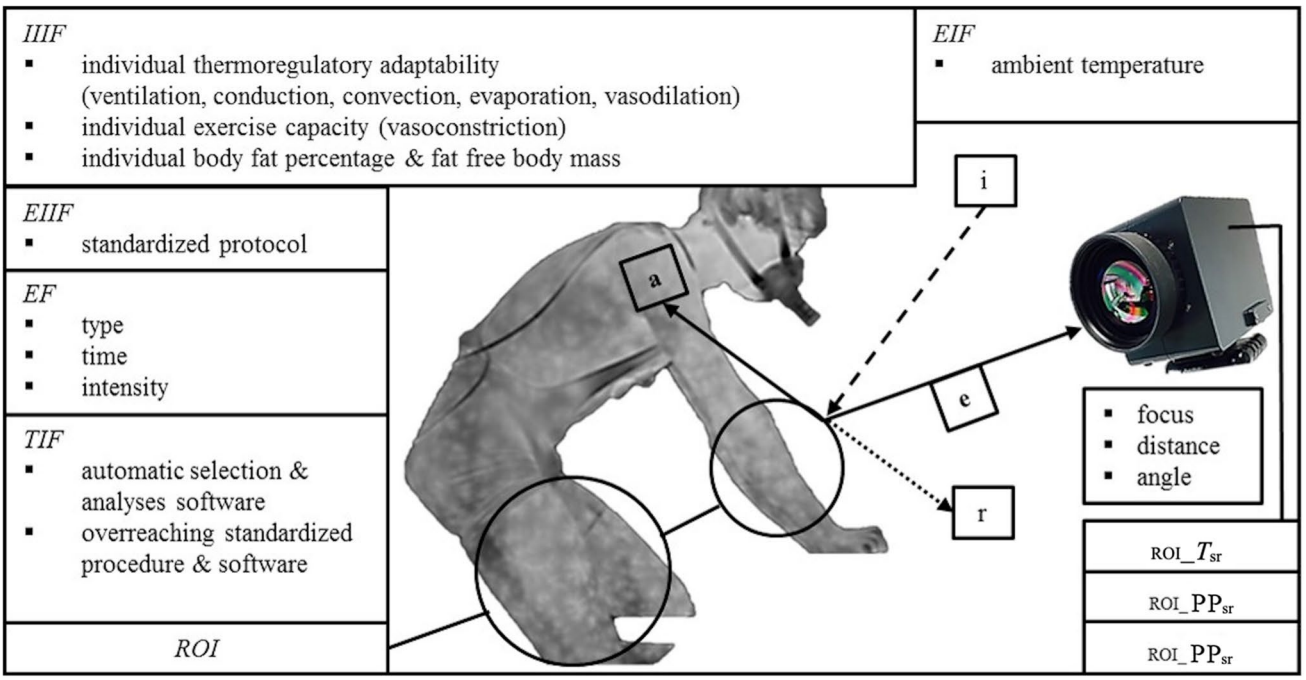

Fig. 6 Summary of the most important influential factors and outcomes for IRT measurements in dynamic exercises (*a* absorption, *i* incoming radiation, *e* emitted radiation, *r* reflected, PP_{sr} perforasome surface radiation pattern, VP_{sr} venous surface radiation pattern, *IIIF* most important internal individual factors, *EIIF* reduction of external individual factors, *EF* specific exercise factor, *TIF* goal for technical influential factors, *EIF* most important environmental influential factor)

The results from the literature and the two demonstrated cases indicate the following: there are inconsistent findings in the literature as to whether *T* increases or decreases during RE, due to methodological and technical heterogeneity. Age, performance levels and exercise execution times can be differentiated with IRT as well as similar contralateral T changes can be measured. Exercise intensity so far seems not to be distinguishable. IRT revealed different P_{sr} compared to EE and XT, which has not been described in the literature for RE so far. These findings can be linked to local and systemic adaptations of cutaneous blood flow specific for RE, which are discussed in Sect. 5.2. Most important is the observation of different P_{sr}, which can explain contradictory study outcomes for RE. Due to these striking P_{sr} differences, neither average T_{sr} nor T_{max} values are valid data that would allow inter-individual and intra-individual comparisons between different body regions or comparisons between studies.

5 Visualization of Thermoregulation, Cutaneous Circulation and Their Related Neuronal Response by IRT

The available literature and our own experiments show that IRT measurement during exercise reveals a dynamic change of T_{sr} and specific kinds of P_{sr} during different types of exercises.

5.1 Temperature Surface Radiation in Constant Load Endurance Exercise and Incremental Exercise Testing

At the onset of EE or XT, all studies reported a measurable decrease in T_{sr}. While a further decline occurred with the incremental increasing intensity in XT, the initial decrease during EE stabilized after a few minutes. This difference of T_{sr} change between EE and XT reveals the dependency of T_{sr} on the intensity of exercise. Therefore, it has been argued that T_{sr} is highly correlated with the sympathetic tone, which is in turn related to the intensity of exercise [39, 40]. More precise, the intensity-dependent decrease of T_{sr} during XT reflects the sympathetic noradrenergic nerve activity, due to the cutaneous arterial vasoconstriction [41, 42]. Thereby, the sympathetic noradrenergic vasoconstrictor nerve, controlled by the rostral medulla oblongata and the preoptic area [42], initiates the release of the neurotransmitters norepinephrine (NE) and neuropeptide Y (NPY), which activate α-adrenergic receptors of cutaneous vascular smooth muscles. Subsequently, this process leads to cutaneous arteriole vasoconstriction [42]. In consequence, there is a redistribution of blood volume to the activated organs [43]. All these processes are needed to adjust the hemodynamic status to fulfill the oxygen requirements of the brain, the heart, and the active muscles during exercise [39]. It

Table 1 Infrared thermography in endurance exercise: overview of included studies

Study	IR camera (pixels)	ROI	Primary IRT outcome	Participants	Exercise type, time, intensity	Results
Tanda [7], 2018	FLIR T335 (320 × 240)	Arithmetic mean of 18 ROI	T_{sk}	$n=4$; 1♀, 3♂; "well trained"	Treadmill running 30 min; 12 km/h	T_{sk} ↓ (− 1.4 °C; 30.6→29.2 °C) ($p<0.05$) (upper limbs: − 2.0, thigh: − 1.0) Slight total T_{sk} ↑ as the exercise progresses (+1.0 °C) T_{sk} ↑ recovery and *"hyper-thermal spots"* (+ 0.8 °C)
Balci et al. [8], 2016	Testo 875-1 ThermaCAM (160 × 120)	Chest and back	T_{sk}, T_{core}	$n=11$; ♂; "moderate to well-trained"	Cycling 20 min 60% VO_{2max}	T_{sk} ↓ until 7.58 ± 1.03th minute, then T_{sk} ↑ until the end T_{core} ↑ ($p<0.05$) "Thermal kinetic pattern"
Fernandes et al. [9], 2016	FLIR T420 (320 × 240)	28 ROI: Forehead, face, chest, abdomen, back, lumbar, anterior, posterior neck, posterior–anterior views of the right and left hands, forearms, upper arms, thighs, and legs	T_{sk}	$n=12$; ♂; "physically active"	Treadmill interval running 1 h; 12 × 5 min 60% VO_{2max} and 1 min break	T_{sk} ↓in most ROI after 10 min ($p\leq0.05$) (legs, anterior hands after 5 min) T_{sk} ↑ after 1 hour of recovery ($p<0.01$) Different in the lower significant increments in the T_{sk} ($p\leq0.05$)
Korman et al. [10], 2016	FLIR SC640 (640 × 480)	Front and back of lower limbs	Surface temperature	$n=8$; ♂; "sprinters"	Endurance training 90 min	Warm-up: surface temperature ↓ − 2.5 °C ($p<0.001$) Surface temperature stabilization until the end (31.3–31.6 °C)
Priego Quesada et al. [11], 2016	FLIR E-760 (320 × 240)	17 ROI: deltoid, chest, abdomen, upper back, lower back, vastus lateralis, rectus femoris, abductor and vastus medialis, biceps femoris, semitendinosus, knee, popliteal, tibialis anterior, gastrocnemius, ankle anterior, Achilles	ΔT; ΔT_{10}; ΔT_{after}	$n=14$; ♂; "cyclists"	Cycling 45 min 35 and 50% of peak power output	T_{core} at 50% = 0.2 and 0.3 °C higher than at 35% ΔT ↓ trunk and tibialis anterior ($p<0.05$), higher at 50% than 35% ($p<0.05$) ΔT ↑ anterior thigh and knee ($p<0.01$)/ ΔT ↔ remaining ROI ΔT10 ↑ trunk, posterior thigh, leg/ ↔anterior thigh and Achilles

Table 1 (continued)

Study	IR camera (pixels)	ROI	Primary IRT outcome	Participants	Exercise type, time, intensity	Results
Tanda [12], 2015	FLIR T335 (320 × 240)	Front and back of the body	T_{sk}	$n=7$; ♀1, ♂6; "healthy and trained runners"	Treadmill running constant load 5 min warm-up 6 km/h 25 min running 12 km/h	T_{sk} ↓ initial stage of running exercise T_{sk} ↑ recovery "Hyperthermal spots" Constant load: followed temperature ↑
Adamczyk et al. [13], 2014	FLIR A325 (320 × 240)	Thighs, forearms, arms, trunk (front and back), behind shins	Body surface T	$n=7$; ♀; "healthy"	Track running 10–12 min	T ↓ (− 1.13 °C behind shoulders/− 0.04 °C trunk) Only shins T ↑ + 0.06 °C Higher VO_{2max} = greater T ↓
Chudecka et al. [14], 2010	ThermaCAM TM Sc500 (320 × 240)	Upper extremities front and back	T_{mean}	$n=16$; ♂; "professional handball players"	Endurance training 90 min	T_{mean} ↓ pre to post T_{mean} ↑ 10 min recovery
Zontak et al. [15], 1998	nk (nk)	Back of the hands	T_{sk}	$n=10$; ♂; "healthy active"	Cycling 20 min constant load 50%; 70%; 90% VO_{2max}	ΔT ↓ until 7th min, then ΔT ↑ until 15th min, then ΔT ↔ until end No difference between 50 and 70% "Dynamic balance between hemodynamic and thermoregulatory processes" Finger temperature ↓ (constant)
Torii et al. [16], 1992	Thermoviewer JTG-500 M (nk)	8 ROI: forehead, upper arms, chest, abdomen, neck	ΔT_{sk}	$n=10$; ♂; "healthy"	Cycling/20 min "moderate" (50–150 W)	T_{sk} ↓ (− 1.5 to 2.0 °C) Increased work intensity = proportional T_{sk} ↓

ROI regions of interest, T_{sk} skin temperature, T_{core} core temperature, T temperature, ΔT difference between temperature immediately after the cycling test and before, $\Delta T10$ difference between temperature 10 min after the cycling test and before, ΔT_{after} difference between temperature 10 min after the cycling test and immediately after; mean T of the upper extremities front and back, *nk* not known, ♀ female, ♂ male, ↓ decrease, ↑ increase, ↔ equal, *ROI* regions of interest

Table 2 Infrared thermography in exercise testing: overview of included studies

Study	IR camera (pixels)	ROI	Primary IRT outcome	Participants	Exercise test	Results
Trecroci et al. [17], 2018	AVIO, TVS-700 (320 × 240)	Anterior thighs	T_{sk}, AI_T, AI_K	$n = 10$; ♂; "elite cyclists"	Incremental cycle test	T_{sk} ↓ ca. − 1.3 °C; basal ($p = 0.008$); starting point ($p = 0.001$)
Tanda [7], 2018	FLIR T335 (320 × 240)	Arithmetic mean of 18 ROI "total body"	T_{sk}	$n = 7$; ♀1, ♂6; "well trained"	Graded treadmill test	T_{sk} ↓ − 1.7; 31.1–29.4 °C (Calves/Thighs − 1; upper limbs − 2.5 °C) ($p < 0.05$) T_{sk} ↑ recovery (+ 0.7 °C) "Hyperthermal spots"
Priego Quesada et al. [18], 2017	FLIR T420 (320 × 240)	Lower limbs, vastus lateralis, rectus femoris, biceps femoris and gastrocnemius	T_{sk}, ΔT_{sk}	$n = 22$; ♂11; "healthy cyclists" (G1); ♂11; "healthy non-cyclists" (G2)	Incremental cycle test	T_{sk} ↓ (-0.6 ± 1.4 °C (VL) 0.6 ± 1.4 °C(RF) − 1.6 ± 1.2 °C (BF) − 1.4 ± 1.0 °C (GM) G1ΔT_{sk}:VL: *VT*1 0.1 (± 0.7) *VT*2 − 0.8 (± 0.6) PO_{peak} – 1.3 (± 1.0) G2ΔT_{sk}: VL: *VT*1 − 0.1 (± 1.4) *VT*2 − 0.5 (± 1.3) PO_{peak} − 0.8 (± 1.3) T_{sk} ↑ (10 min recovery) $r = -0.5$ T_{sk}/body fat % ($p < 0.05$) (G1 = lower body fat % ($p < 0.01$) $r = 0.5$ ΔT_{sk} (GM)/PO_{peak} ($p < 0.05$) G1: higher T_{sk} knee extensors and higher VO_{2max} ($p < 0.01$)
Balci et al. [8], 2016	Testo 875-1 Therma CAM (160 × 120)	Chest and back	T_{sk}, T_{core}	$n = 11$; ♂; "moderate to well trained"	Incremental cycle test	T_{sk} ↓ T_{core} ↑ ($p < 0.05$)
Ludwig et al. [19], 2016	AVIO TVS700 (320 × 240)	Frontal thigh	T_{max}	$n = 7$; ♂; "cyclists"	Incremental cycle test	T_{sk} ↓ (32.5 °C to 30.9 °C) T_{sk} ↑ recovery ($p < 0.01$) + "*hot-spotted thermal pattern*"
Duc et al. [20], 2015	FLIR SC1000 (256 × 256)	Quadriceps and calves	T_{sk}, ΔT	$n = 7$; ♂; "trained cyclists"	Incremental cycle test	T_{sk} ↓ VL/GM muscle (− 2.6/2.7 ± 0.6 °C) $r = -0.8$ T_{sk}VL/Hr ($p < 0.001$); $r = -0.77$ ΔT GM/Hr ($p < 0.001$) $r = 0.72$ T_{sk}VL/VO_2 ($p < 0.001$); $r = -0.64$ ΔT GM/VO_2 ($p < 0.001$)

Table 2 (continued)

Study	IR camera (pixels)	ROI	Primary IRT outcome	Participants	Exercise test	Results
Priego Quesada et al. [21], 2015	FLIR E60 (320 × 240)	Rectus femoris, vastus lateralis, biceps femoris and gastrocnemius medialis	ΔT, ΔT10, ΔT_{after}	$n = 10$; (nk); "physically active"	Incremental cycle test	ΔT_{sk} Knee extensors ↑ (0.9–2.0 °C); Vastus lateralis (0.9–2.3 °C) $r = -0.7$ skinfold/ ΔT VL and RF ($p < 0.01$)
Arfaoui et al. [22], 2014	FLIR SC1000 (256 × 256)	Gastrocnemius	T_{sk}	$n = 11$; ♂; "master cyclists"	Incremental cycle test	T_{sk}↓ (according to power output level) T_{sk} 150 ≠ 200 W ($p = 0.016$) $r = 0.99$ ΔT_{sk}/HR ($p < 0.0001$) *"Hyperthermal spots"* (perforator vessels)
Akimov and Son'kin [23], 2011	NEC TH9100 (nk)	Forehead	T	$n = 20$; ♂; "athletes"; 2/3 = "endurance athletes"; 1/3 = "various sport"	Incremental cycle test	1st: T↓, followed by T↑ until exhaustion; 2nd: T↓; working capacity: 1st = 2nd 1st: 4 mmol/l lactate threshold corresponded to T↑ 2nd: lactate threshold corresponded to T↓
Merla et al. [24], 2010	FLIR (320 × 240)	Anterior cutaneous temperature	T_c	$n = 15$; ♂; "well trained"	Graded treadmill test	Tc ↓ (ø − 3–5 °C) (thighs and forearms = earliest ↓) Tc ↑ recovery (thighs and forearms = earliest ↑) *"Hyperthermal spots"* (perforator vessels)
Akimov et al. [25], 2010	NEC TH 9100SL (nk)	Upper back (dorsum)	T_{sk}	$n = 53$; ♂; "healthy"	Treadmill ramp test or Incremental cycle test	$r = 0.6$ T_{sk} (rest)/maximal aerobic capacity ($p < 0.05$) $r = -0.7$ T_{sk} (rest)/ lactate level (after 10 min recovery) ($p < 0.05$)
Akimov et al. [26], 2009	NEC TH 9100SL (nk)	Upper back "all back surface" (ABS)	ABS T_{sk} (min, max, ø)	$n = 40$; ♂; "sportsmen"	Graded treadmill test	$r = 0.69$ minABS T_{sk}/VO_{2max} and $r = 0.051$ maxABS T_{sk}/VO_{2max} $r = 0.63$ AT_VO_2/ øABS T_{sk}

T_{sk} skin temperature, T temperature, AI_T asymmetric index temperature, AI_K asymmetric index kinetic, *nk* not known, *ROI* regions of interest, ΔT_{sk} difference between temperature immediately after the test and before, ΔT difference between temperature immediately after the cycling test and before, $\Delta T10$ difference between temperature 10 min after the cycling test and before, ΔT_{after} difference between temperature 10 min after the cycling test and immediately after, T_c cutaneous temperature, ♀ female, ♂ male, ↓ decrease, ↑ increase, ↔ equal, G1 Group 1, G2 Group 2, PO_{peak} peak power output, *AT* VO_2 VO_2 at anaerobic threshold, $ABST_{sk}$ all back surface skin temperature, *RF* rectus femoris, *VL* vastus lateralis, *BF* biceps femoris, *GM* gastrocnemius medialis

Table 3 Infrared thermography in resistance exercise: overview of included studies

Study	IR camera (pixels)	ROI	Primary IRT outcome	Participants	Exercise type, time, intensity	Results
Weigert et al. [28], 2018	FLIR A35 (nk)	Biceps brachii	T	$n=10$; ♂; "healthy"	Biceps curl 3 × 10 rep. 2 min rest 30%; 50%; 70% of 1RM	T ↑ (ave. 1.8 °C) independent of the intensity T peak 5 min after 3rd set Homogeneous T pattern
Silva et al. [29], 2017	FLIR (320 × 240)	Thigh, forehead	T_{sk}	$n=38$; ♀33, ♂5; "mixed active"; G1: 9, G2: 10, G3: 9 G4: 10	G1: 15 min (running) 80% HR G2 and G3: plyometric squat jumps (body weight) 5 × 20 rep/ 2 min rest G4: CG	G2 and G3 T_{sk} ↑ T_{sk} G2 and G3 > G1
Sillero-Quintana et al. [30], 2017	FLIR T335 (nk)	Thigh (external, internal, central, adductor), knee	T_{sk}	$n=17$; ♂; G1: "high-trained", G2: "Low-trained"	Unilateral leg press and knee extension 4 × 10 rep/ 90 s. Rest 2 s. eccentric ↔ concentric Leg press 70% Knee extension 50% of 1 RM	T_{sk} ↑; T_{sk} peak 30 min after exercise Low ≠ high-trained for all ROI except for the anterior knee: post-training, 30-min and 60-min post-training in the nonexercised limb Contralateral T_{sk} ↑
Neves et al. [31], 2016	Fluke (320 × 240)	Thigh, biceps brachii	T_{sk}	$n=31$; ♀; "untrained"	(a) unilateral biceps curl (b) back half squat 4 × 10 rep/ 30 s. rest (a) 70% and 85% (b) 90% of 1RM	T_{sk} ↓ for a) and b) → 15 min (standing) 70% = 85%
Formenti et al. [32], 2016	AVIO TVS 700 (320 × 240)	Thigh	T_{max}	$n=13$; ♂; "active"	Squat (50% of 1RM until exhaustion) (a) max rep 1 s concentric ↔ eccentric (b) 5 s concentric ↔ eccentric	T_{max}↓ T_{max}↓ more slowly in b ($p=0.002$) ΔT: $a=b$
Neves et al. [33], 2015	FLIR (320 × 240)	Biceps brachii	T_{sk}	$n=13$; ♂; "trained"	Biceps curl/hammer curls dominant arm 5 × 8 rep.; 1 s.: concentric ↔ eccentric rest 90 s. 70% of 1RM	T_{sk} ↑ 24–96 h post-exercise T_{sk} and muscle thickness 24–96 h post-exercise ($r=0.9$; $p=0.017$)
Adamczyk et al. [34], 2014	MobIR M3 (160 × 120)	Lower limbs, front and back surface	T_{sk}	$n=16$; ♂; "non-trained"	Squat jumps (body weight); 1 min 30 min sitting recovery	Front and back surface: $r=0.83$, ($p<0.05$) T_{sk} ↓ (ø − 1.44 °C) ($p<0.001$) T_{sk} ↑ recovery period

Table 3 (continued)

Study	IR camera (pixels)	ROI	Primary IRT outcome	Participants	Exercise type, time, intensity	Results
Formenti et al. [35], 2013	AVIO TVS 700 (320 × 240)	Calves	T_{max}	$n=14$; ♀; G1 "trained", G2 "untrained"	Standing heels raise 2 min 1 s eccentric ↔ concentric Ca. 60 rep.	T ↑ G1 ≠ G2 (ø: +1 °C ≠ +0.4 °C) G1 T_{sk} ↑ more quickly ($p<0.05$)
Al-Nakhli et al. [36], 2012	FLIR 660 (nk)	Biceps brachii	T_{sk}	$n=41$; (nk)	Unilateral biceps curls 4 × 25 reps /rest 90 s. 35% of 1RM	T_{sk} ↑ pre to 24 h post (ø +1.1 °C) ($p<0.01$) active = passive arm
Ferreira et al. [37], 2008	Fermionics Opto Tech. (nk)	Thigh (posterior)	T_{sk}	$n=29$; ♀ 22, ♂ 7, 14: "Elderly" (67 ± 5 years), and 15: "young" (23 ± 2 years)	Knee flexion 3 min 1 kg	Elderly ≠ young subjects pre-exercise ($p<0.01$) T_{sk} ↔ "displayed heat concentration in exercised areas" T_{sk} ↓ young: 10-min post-exercise (30.7 ± 1.7 to 30.3 ± 1.5 °C; ($p<0.05$)) T_{sk} ↓ post-exercise ($p<0.01$) in the contralateral limb for both groups
Coh and Sirok [38]	CMT384SM (nk)	Thigh	Skin surface T	$n=1$; ♂; "trained"	"Sprint different loads" 9 series	Increased loading = skin surface T ↑ Increased loading = "more homogeneous temperature field"

♀ female, ♂ male, ↓ decrease, ↑ increase, ↔ equal, *G1* group 1, *G2* group 2, *1RM* one repetition maximum

has been discussed that IRT rather detects the vasomotor adjustments than changes in evaporation, since the vasomotor adjustments remain the preferred economic choice of the body to deal with the increase of internal heat [42, 44]. Therefore, IRT may preferentially reflect the vasomotor changes with the onset of EE and intensity increases during XT, without being profoundly influenced by evaporation. The progressive occurrence of a vessel-shaped P_{sr} supports this idea as we will now explain.

Prolonged exercise provokes an increasing heat production in the active organs, and the thermal equilibrium of core temperature of roughly 37 °C is going to increase [44]. Whereas T_{sr} further decreases (XT) or remains stable (EE), we show here that high-resolution IRT reveals an increasing P_{sr} (Figs. 1, 2). The P_{sr} indicates two pathways of cutaneous vascular adaptation to prolonged exercise. One pathway is the previously described NE- and NPY-induced cutaneous arteriole vasoconstriction [42]. The second pathway is the reflex neurogenic vasodilation due to an increased internal and exercising tissue temperature [45]. If the internal or deep tissue temperature in the exercising muscle exceeds a specific level, the cholinergic nerve transmission activates the non-adrenergic vasodilator system [45]. This leads to active vasodilation of the vessels in the vascular bed of the skin [41, 45].

The emerging P_{sr} in EE and XT, therefore, mirrors the increasing systemic heat dissipation due to increasing core temperature. It was claimed that the tree-shaped P_{sr} represents perforator vessels [22, 24]. These perforator vessels increase the heat dissipation by way of intensified vascular convective heat transfer and higher vascular conduction to the skin surface. These observations are similar to earlier findings in which reflex neurogenic vasodilation was measured via bloodflowmetry during exercise. For example, Kellog et al. [46] found that reflex neurogenic vasodilation starts to increase when the core temperature rises about 0.2–0.3 °C during exercise and the skin temperature to 38 °C. Additionally, this research group has shown that reflex neurogenic vasodilation was immediately increased by a skin temperature of 38 °C under resting conditions. Taken together, these findings suggest the threshold for reflex neurogenic vasodilation is delayed during exercise. The observations of our case experiment in exercise testing (Fig. 2) further lead to the assumption that there is a significant local delay of reflex neurogenic vasodilation threshold over active muscles (thigh), but simultaneously there is only a slight delay of reflex neurogenic vasodilation threshold in blood vessels over inactive limbs (forearm, chest) during cycling.

Furthermore, most studies reported an immediate increase of P_{sr} directly at the end of exercise [7] (Fig. 2). It is highly likely that IRT reveals the vasodilation of cutaneous perforator vessels as a consequence of an immediately decreased sympathetic tone directly after exercise. Additionally, decreased sympathetic tone also leads to increased perfusion of the constricted cutaneous arterioles, which is in line with the increase in T_{sr} observed by most EE and all XT studies.

In plastic surgery, research has been conducted on the localization and anatomy of perforating vessels [47–50]. The skin consists of the surface, the epidermis and the dermis [51]. The dermis contains the blood vessels of the dermal papillae (sub-papillary network) and the dermal plexus (arterioles, venules, deep vascular network) [51]. This layer is about 1–1.5 mm below the skin surface [52]. Below, in the "dermal-subdermal junction", are the blood vessels of the subdermal plexus [51, 52]. The respective layers of the plexuses are interconnected [53]. The blood vessels of the subdermal plexus are the perforator vessels that become detectable by IRT during EE and XT and they originate from the adjacent musculature and the underlying fatty tissue [47, 52]. These vessels run perpendicular to the skin [47]. Liu et al. [54] estimate this vascular plexus at a depth of about 10 mm. Heating in such a depth would only becomes visible by convection and conduction with IRT. Saint- Cyr et al. [49] showed that the perforator vessels originating from a source artery penetrate the deep fascia reaching out for the skin surface, while progressively branching to all sides. This entire structure is called a "perforasome". The perforasomes form a vascular network via connecting vessels that extends over the entire body [50]. Based on this, the P_{sr} appearing during EE and XT can be specified as "perforasome surface radiation pattern" (PP_{sr}) (see Fig. 5, left).

5.2 Venous, Homogeneous, and Perforasome Surface Radiation Pattern in Resistance Exercise

For the first time, we indicate that IRT can detect three different ways to dissipate heat during RE. One way is preferentially observed over the muscle surface of larger muscle groups (venous P_{sr}), one over the surface of smaller muscle groups (homogeneous P_{sr}) and a third last perforasome surface radiation pattern (PP_{sr}). In the following paragraphs, we will discuss the physiological concepts of how these three pattern types develop.

The venous P_{sr} (see Fig. 5, middle) develops on the basis of three factors that lead to preferential heat dissipation from the superficial veins over the working muscle involved. First, the increase of heat production in active muscles is related to the metabolic ATP production and can be more than doubled during high-intensity exercises [44]. Second, this local increase in a large working muscle is primarily dissipated via convection through the blood transported by the superficial veins, since heavy load exercise leads to a redistribution of blood from deep to superficial veins. Third, the venous return from the working muscle is reduced due to exercise, which increases the internal muscle temperature and favors conduction of heat from the superficial veins through the

overlaying skin and radiation from the skin parts over the superficial veins (Fig. 3). This acute adjustment to dissipate heat more efficient is also influenced by the amount of included muscle mass [44].

We found a homogeneous P_{sr} (see Fig. 5, right) in heavy exercises, which involve smaller muscles on a smaller body region. The heat seemed to be primarily homogeneously radiated from the skin surface. In the example of the shoulder muscle (Fig. 4), the muscle volume to muscle surface relationship is profoundly shifted towards the surface, leading to a higher conduction of heat directly from the working muscle to the overlaying skin surfaces. Moreover, the more homogeneous radiation of heat directly above the muscle (Fig. 4) could be related to a high shear-stress per volume of muscle mass, which is more likely to occur in smaller muscle groups with high fast-twitch fiber proportion subjected to heavy load. Additionally, venous return of blood from the muscle is reduced and the local heat has to be transferred via superficial blood vessels, away from the working smaller muscle groups.

In the knee-extension experiment with P1, a slight PP_{sr} is also visible post-exercise (Fig. 3). As already mentioned in Sect. 5.1, PP_{sr} could be most likely triggered due to an increased venous blood temperature, which eventually exceeds the core temperature [44]. A consequent core temperature rise of 0.2–0.3 °C leads to the activation of the non-adrenergic vasodilator system [46]. This activation of the reflex neurogenic vasodilation could be mirrored by the PP_{sr} over the active and the inactive muscle surface (Fig. 3).

An alternative explanation would be that the slight PP_{sr} reaction is occurring because of an increase in epinephrine and norepinephrine that can be expected when a larger muscle mass is subjected to high-repetition RE [55]. In either view, it becomes clear that the appearance of PP_{sr} most likely reflects systemic activation during RE, especially since it is in contrast to venous P_{sr}, not restricted to the vicinity of the exercising part of the body, but also occurs on the contralateral leg (Fig. 3).

The IRT findings appear physiologically transferable and promising, but have to be considered carefully due to the limited number of studies and, in particular, other influential factors (see next section).

6 Separating Influential Factors from Physiological Traits in Dynamic Exercises

Influential factors (IF) are considered as a critical issue for exercise-related IRT measurement. Most common IF-caused problems are the reproducibility of thermograms, the inter-individual comparison and the validity of IRT-related diagnostic outcomes [4, 56–59]. This section is about the most significant exercise-related bias here termed IF. Given that the vast majority of studies measure T_{sk} in this section, we shall firstly discuss its validity and secondly propose alternatives that may turn out to be more precise due to their potential robustness against IF.

6.1 "Skin Temperature" (T_{sk}) or Another Parameter?

At first, most of the previously described investigations measured the parameter average skin temperature of a specific ROI to describe the IRT-related outcome. However, there are serious indications to avoid the term T_{sk}. IRT detectors measure the surface radiation of objects [60]. Thermal radiation in physics can be correlated via the Planck law to a surface temperature measured in Kelvin (K) [60]. This object-emitted radiation (e) contributes to the absorption (a) of a detector and is the deviation of incoming radiation (i) minus the reflection (r) ($e = a = i - r$) [61]. This emitted radiation is affected by IF, especially in humans [4]. Furthermore, the detection of emitted radiation by IRT detectors typically leads to lower values than the real skin temperature [61]. The detected radiation is not the real T_{sk} of humans, but rather a mixture of environmental radiation and human surface radiation [62]. Thus, compared to T_{sk}, a parameter such as T_{sr} of a specific ROI might be a more precise term. To describe the commonly observed *"hot thermal spots"* more precisely, surface radiation pattern (P_{sr}) is recommended by the authors.

6.2 Important Influential Factors

The mentioned IF can be categorized into environmental, technical internal individual and external individual influential factors [4].

Environmental influential factors are subcategorized into room size, ambient temperature, relative humidity, atmospheric pressure, and source radiation. However, room size can be combined with ambient temperature, due to its direct influence. Relative humidity and atmospheric pressure is the sum of CO_2, ozone, and steam [61]. The influence is relatively low, because of the short distance (− 10% by 100 m distance) between the camera and the test subjects ($\leq$ 5 m) [61]. More important is that T_{sr} is defined as object radiation plus atmospheric radiation [61]. Thus, a background with low emissivity and less other source radiation is advisable. Nevertheless, usually, the influence of the background is low (5%), due to the high emissivity of human skin (0.98) [61]. Moreover, the ambient temperature has a significant impact on thermograms and is attributable to the essential environmental influential factor [63]. It has been shown that the superficial radiation of humans increases proportionally to the ambient temperature [63]. Most of the IRT observations resulted in a temperature increase or decrease of 0.1–2 °C

ΔT. This could also be implicated by an increased or decreased ambient temperature during the IRT measurement. To neglect or monitor this bias, a static IRT detectable control object, besides the test person, should be applied [61]. Furthermore, the influence of draught, due to the fast leg or arm movement, depending on various types of exercise, has to be taken into account [63].

External individual influential factors are intake factors (medications, drinks and food), skin applications, therapies and physical activity. The effects of external individual influential factors are easy to reduce by avoiding these factors before IRT measurements. The real and exact influences of most internal individual influential factors remain unclear due to a lack of investigations [64–69]. Sex, age, anthropometry, genetic, medical history, and metabolic rate have a collective influence on skin blood flow itself. Thus, skin blood flow can be seen as the sum and the result of changing internal individual factors, which greatly complicates inter-individual comparisons for dynamic exercise diagnostics [56]. In addition to skin blood circulation, previous studies have shown that the influence of the body fat percentage and the fat-free mass must also be seen as a strong influencing factor [65, 70]. Moreover, skin blood flow is also affected by the physiological adaptation to increasing or decreasing core temperature and different exercise modalities [45].

According to the blood flow adjustments to physical strain and thermoregulatory needs, a fourth factor, the exercise factor, must be considered. This factor consists of exercise time, type and intensity. As mentioned above, different types of exercise, intensity, and time lead to specific skin blood flow adjustment. Theoretically, the longer and more intensive the exercise, the higher is the mechanical and metabolic heat production. This leads to a stronger thermoregulatory adaptation and similar to more pronounced vasoconstriction of cutaneous arterioles. An increased influence on the T_{sr} or P_{sr} is apparent and needs to be differentiated precisely and examined in the following investigations. Thus, it will be possible to predict a specific exercise-related IRT outcome in future.

Technical influential factors are composed of validity, reliability (accuracy and precision), recording protocol, camera features, ROI selection, analysis software, and statistical analysis. Moreira et al. [71] recommend a camera with the highest possible resolution and a standardized measurement protocol. Additionally, a camera-to-ROI angle lower than 30°, and an exact and stable focus must be ensured, which will finally lead to a well-defined and reproducible spatial resolution [61]. While this is easier to implement, the ROI selection and improvement of the analysis software are the current critical issues for IRT research in dynamic exercise. For the analysis of radiation data during dynamic exercise, there are currently various possibilities to determine the ROI. For example, a researcher can either use a ROI close to the stressed muscles or in a peripheral area of the body. As illustrated in Fig. 2, the IRT outcome differs even in one subject concerning different ROI selection in one exercise setting. Similar findings have been discussed by Maniar and Bach [72] and Quesada et al. [27] in an examination of different ROIs. An overview of the influential factors is illustrated in Fig. 6.

Currently, some methods are discussed for the analysis of different ROIs in static body positions [73–76]. A manual ROI selection (geometric shape) was mostly applied, which appears inaccurate because of the specific anatomical shape of humans' extremities, leading to a loss of and incomparability of data. Fournet et al. [73] conducted a trial about morphing and segmentation of ROIs, regardless of the anthropometry, before and after physical strain. In addition, Duarte et al. [74] applied different segmentation methods and a displacement field for the comparison of thermograms. These authors investigated the possibility of choosing a ROI independently of its geometric shape. This automatic ROI selection resulted in a loss of information about minimum temperature pixel, due to the naturally rounded body shape. Barcelos et al. [76] examined a new threshold segmentation for improved automatic detection of body silhouettes and isotherms in greyscale thermograms. This approach has successfully demonstrated the possibility to compare different thermograms of one person throughout successive training sessions. However, there is a lack of studies examining the analysis strategies for different ROIs, even though this is the essential component to fulfill the quality criteria for future IRT diagnostics.

7 Future Directions

Consequently, to generate reliable and comparable outcomes, the specific exercise-type-ROI has to be examined and defined. This ROI should be analyzed comprehensively. Uniform analysis software for thermograms of different dynamic exercises is urgently needed. This software should automatically detect and sensitively distinguish T_{sr}, PP_{sr} and venous P_{sr} as well as other skin surface temperature variations, for example, the heating of skin on top of muscle or connective tissue due to convection. This cornerstone could be achieved with software, using different segmentation methods, automatic image recognition, and observer-independent automatic ROI selection. For instance, Unger et al. [77] demonstrated an algorithm for the automatic detection of perforator vessels and showed the individual anatomy of blood vessels. Deng and Liu [78] investigated possibilities to distinguish between different P_{sr} from a "thermographic signal reconstruction algorithm". Additionally, future research should be related to the experience of medical IRT research. Cheng et al. [79] used three-dimensional thermal imaging

for biological surfaces to obtain more information about size, color, and temperature of the skin surface. Moreover, Deng and Liu [80] applied mathematical modeling of temperature mapping over the skin surface. Recently examined analyses methods, such as augmented reality [81] or dynamic infrared thermography [82], deep learning [83] and in particular radiomics [6], should also be taken into account.

Radiomics is defined as the conversion of digital radiologic images into mineable high-dimensional data with the great potential to accelerate precision medicine [6]. The extensive datasets of pictures were analyzed via pattern recognition tools and provided information that reflects underlying pathophysiology and improves diagnostic, prognostic and predictive accuracy [6]. The original concept uses quantitative image features based on intensity, shape, size or volume, and texture to offer information on tumor phenotype [6]. Digital radiologic and thermographic pictures are different, but the processing of the thermographic pictures can be executed similarly. The implied steps are acquiring the images, identifying the ROI, segmenting the ROI, extracting and qualifying characteristic features from the ROI, using these to populate a searchable database, and mining these data to develop classifier data and predict outcomes, or combine them with additional data of the individual [6]. The improved, comprehensive and high-quality analyses would enhance the significance of IRT concerning acute neuronal and cardiovascular adaptation as well as long-term physiological function.

8 Conclusion: Performance-Related IRT Measurements in Sports—More Than a Sleeping Beauty?

IRT can principally display acute physiological adaptations to exercise. Thus, specific characteristics can be detected for different types of exercise. A change of the T_{sr} occurs in EE, XT and is somehow inconsistent in RE. In particular, the T_{sr} change during EE and XT seems to be related to the sympathetic noradrenergic nerve activity and is recognizable by the IRT due to the cutaneous arterial vasoconstriction.

Furthermore, IRT seems to visualize the reflex neurogenic vasodilation of perforator vessels to enhance heat dissipation, leading to a tree-shaped PP_{sr}. IRT in RE displays acute local and systemic adjustments of the cutaneous circulation. In contrast to EE and XT, the heat dissipation is mostly regulated by superficial veins in RE. The magnitude of these adjustments is mainly dependent on the type, time, and intensity of exercise in combination with individual prerequisites and the environmental conditions.

Acute reactions and long-term adaptations of the PP_{sr} in exercise physiology have not yet been investigated. Such alterations of the PP_{sr} may relate to factors associated with the individual performance level, training adaptation, thermoregulatory capacity, core temperature and fatigue. Furthermore, the PP_{sr} may help to adjust or monitor individual training load.

There are influential factors that limit the potential of IRT. Some can be reduced by standardization. However, the most substantial limitations are insufficient analysis strategies that reduce the accuracy, objectivity, reliability, and validity of the datasets. To overcome these limitations, a software that automatically detects T_{sr}, PP_{sr}, and venous P_{sr} should be developed, including improved algorithms and automated data processing. Thereby, innovative technologies such as artificial intelligence, deep learning and radiomics should be taken into account to enable a comprehensive, uniform data analysis.

Acknowledgements The authors thank the participants for their voluntary participation in the case experiments.

Compliance with Ethical Standards

Funding No sources of funding were used to assist in the preparation of this article.

Conflict of interest Barlo Hillen, Daniel Pfirrmann, Markus Nägele, and Perikles Simon declare that they have no conflicts of interest relevant to the content of this review.

References

1. Lahiri BB, Bagavathiappan S, Jayakumar T, Philip J. Medical applications of infrared thermography: a review. Infrared Phys Technol. 2012;55:221–35.
2. Hildebrandt C, Zeilberger K, John Ring EF, Raschner C. The application of medical infrared thermography in sports medicine. An Int Perspect Top Sport Med Sport Inj. 2012, pp 257–274. Available from: http://www.intechopen.com/books/an-international-perspective-on-topics-in-sportsmedicine-and-sportsinjury/the-application-of-medical-infrared-thermography-in-sports-medicine.
3. Lasanen R. Infrared thermography in the evaluation of skin temperature: Applications in musculoskeletal conditions. 2015;103.
4. Fernández-Cuevas I, Bouzas Marins JC, Arnáiz Lastras J, Gómez Carmona PM, Piñonosa Cano S, García-Concepción MÁ, et al. Classification of factors influencing the use of infrared thermography in humans: a review. Infrared Phys Technol. 2015;71:28–55.
5. Nybo L, Rasmussen P, Sawka, MN. Performance in the heat-Physiological factors of importance for hyperthermia-induced fatigue. Compr Physiol. 2014;4:657–89.
6. Gillies RJ, Kinahan PE, Hricak H. Radiomics: images are more than pictures, they are data. Radiology. 2016;278:563–77.
7. Tanda G. Total body skin temperature of runners during treadmill exercise: a pilot study. J Therm Anal Calorim. 2018;131:1967–77.
8. Balci GA, Basaran T, Colakoglu M. Analysing visual pattern of skin temperature during submaximal and maximal exercises. Infrared Phys Technol. 2016;74:57–62.
9. Fernandes A de A, Amorim PR dos S, Brito CJ, Sillero-Quintana M, Marins JCB. Regional skin temperature response to moderate

aerobic exercise measured by infrared thermography. Asian J Sports Med. 2016;7:1–8.
10. Korman P, Straburzyńska-Lupa A, Kusy K, Kantanista A, Zieliński J. Changes in body surface temperature during speed endurance work-out in highly-trained male sprinters. Infrared Phys Technol. 2016;78:209–13.
11. Priego Quesada JI, Martínez N, Salvador Palmer R, Psikuta A, Annaheim S, Rossi RM, et al. Effects of the cycling workload on core and local skin temperatures. Exp Therm Fluid Sci. 2016;77:91–9.
12. Tanda G. The use of infrared thermography to detect the skin temperature response to physical activity. J Phys Conf Ser. 2015;655.
13. Adamczyk JG, Educ P, Bia D. Usage of thermography as indirect non- invasive method of evaluation of physical efficiency. Pilot study. Pedagog Psychol Med Biol Probl Phys Train Sport. 2014;90–5.
14. Chudecka M, Lubkowska A. Temperature changes of selected body's surfaces of handball players in the course of training estimated by thermovision, and the study of the impact of physiological and morphological factors on the skin temperature. J Therm Biol. 2010;35:379–85.
15. Zontak A, Sideman S, Verbitsky O, Beyar R. Dynamic thermography: analysis of hand temperature during exercise. Ann Biomed Eng. 1998;26:988–93.
16. Torii M, Yamasaki M, Sasaki T, Nakayama H. Fall in skin temperature of exercising man. Br J Sports Med. 1992;26:29–32.
17. Trecroci A, Formenti D, Ludwig N, Gargano M, Bosio A, Rampinini E, et al. Bilateral asymmetry of skin temperature is not related to bilateral asymmetry of crank torque during an incremental cycling exercise to exhaustion. PeerJ. 2018;6:e4438.
18. Priego Quesada JI, Sampaio LT, Bini RR, Rossato M, Cavalcanti V. Multifactorial cycling performance of cyclists and non-cyclists and their effect on skin temperature. J Therm Anal Calorim. 2017;127:1479–89.
19. Ludwig N, Trecroci A, Gargano M, Formenti D, Bosio A, Rampinini E, et al. Thermography for skin temperature evaluation during dynamic exercise: a case study on an incremental maximal test in elite male cyclists. Appl Opt. 2016;55:D126. A.
20. Duc S, Arfaoui A, Polidori G, Bertucci W. Efficiency and thermography in cycling during a graded exercise test. J Exerc Sport Orthop. 2015;2:01–8.
21. Priego Quesada JI, Carpes FP, Bini RR, Salvador Palmer R, Pérez-Soriano P, Cibrián Ortiz de Anda RM. Relationship between skin temperature and muscle activation during incremental cycle exercise. J Therm Biol. 2015;48:28–35.
22. Arfaoui A, Bertucci WM, Letellier T. Thermoregulation during incremental exercise in masters cycling. J Sci Cycl. 2014;3:32–40.
23. Akimov EB, Son'kin VD. Skin temperature and lactate threshold during muscle work in athletes. Hum Physiol. 2011;37:621–8.
24. Merla A, Mattei PA, Di Donato L, Romani GL. Thermal imaging of cutaneous temperature modifications in runners during graded exercise. Ann Biomed Eng. 2010;38:158–63.
25. Akimov EB, Andreev RS, Kalenov YN, Kirdin AA, Son'kin VD, Tonevitsky AG. The human thermal portrait and its relations with aerobic working capacity and the blood lactate level. Hum Physiol. 2010;36:447–56.
26. Akimov EB, Andreev RS, Arkov VV, Kirdin AA, Saryanc VV, Sonkin VD, et al. Thermal "portrait" of sportsmen with different aerobic capacity. Acta Kinesiol Univ Tartu. 2012;14:7.
27. Priego Quesada JI, Lucas-Cuevas AG, Salvador Palmer R, Pérez-Soriano P, Cibrián Ortiz De Anda RM. Definition of the thermographic regions of interest in cycling by using a factor analysis. Infrared Phys Technol 2016;75:180–6.
28. Weigert M, Nitzsche N, Kunert F, Lösch C, Baumgärtel L, Schulz H. Acute exercise-associated skin surface temperature changes after resistance training with different exercise intensities. Int J Kinesiol Sport Sci. 2018;6:12.
29. Silva YA, Santos BH, Andrade PR, Santos HH, Moreira DG, Sillero-Quintana M, et al. Skin temperature changes after exercise and cold water immersion. Sport Sci Health. 2017;13:195–202.
30. Sillero-Quintana M, Brito CJ, Adamczyk JG, Estal-Martínez A, Escamilla-Galindo VL, Arnaiz-Lastras J. Skin temperature response to unilateral training measured with infrared thermography. J Exerc Rehabil. 2017;13:526–34.
31. Neves EB, Cunha RM, Rosa C, Antunes NS, Felisberto IMV, Vilaça-Alves J, et al. Correlation between skin temperature and heart rate during exercise and recovery, and the influence of body position in these variables in untrained women. Infrared Phys Technol. 2016;75:70–6.
32. Formenti D, Ludwig N, Trecroci A, Gargano M, Michielon G, Caumo A, et al. Dynamics of thermographic skin temperature response during squat exercise at two different speeds. J Therm Biol. 2016;59:58–63.
33. Neves EB, Moreira TR, Lemos R, Vilaça-Alves J, Rosa C, Reis VM. Using skin temperature and muscle thickness to assess muscle response to strength training. Rev Bras Med do Esporte. 2015;21:350–4.
34. Adamczyk JG, Boguszewski D, Siewierski M. Thermographic evaluation of lactate level in capillary blood during post-exercise recovery. Kinesiology. 2014;46:186–93.
35. Formenti D, Ludwig N, Gargano M, Gondola M, Dellerma N, Caumo A, et al. Thermal imaging of exercise-associated skin temperature changes in trained and untrained female subjects. Ann Biomed Eng. 2013;41:863–71.
36. Al-Nakhli HH, Petrofsky JS, Laymon MS, Berk LS. The Use of thermal infrared imaging to detect delayed onset muscle soreness. J Vis Exp. 2012;1–9.
37. Ferreira JJA, Mendonça LCS, Nunes LAO, Andrade Filho ACC, Rebelatto JR, Salvini TF. Exercise-associated thermographic changes in young and elderly subjects. Ann Biomed Eng. 2008;36:1420–7.
38. Čoh M, Širok B. Use of the thermovision method in sport training. Phys Educ Sport. 2007;5:85–94.
39. Just TP, Cooper IR, DeLorey DS. Sympathetic vasoconstriction in skeletal muscle: adaptations to exercise training. Exerc Sport Sci Rev. 2016;44:137–43.
40. O'Leary D, Silva BM, Marongiu E, Crisafulli A, Piepoli MF, Nobrega ACL. Neural regulation of cardiovascular response to exercise: role of central command and peripheral afferents. Biomed Res Int. 2014;2014:1–20.
41. Charkoudian N. Mechanisms and modifiers of reflex induced cutaneous vasodilation and vasoconstriction in humans. J Appl Physiol. 2010;109:1221–8.
42. Ootsuka Y, Tanaka M. Control of cutaneous blood flow by central nervous system. Temperature. 2015;2:392–405.
43. Williamson JW. Autonomic responses to exercise: where is central command? Auton Neurosci Basic Clin. 2015;188:3–4.
44. Gonzales-Alonso, J. Symposium Report. Human thermoregulation and the cardiovascular system. A key but little understood function of the cardiovascular system is to exchange heat between. 2012;3:340–6.
45. Demachi K, Yoshida T, Kume M, Tsuji M, Tsuneoka H. The influence of internal and skin temperatures on active cutaneous vasodilation under different levels of exercise and ambient temperatures in humans. Int J Biometeorol. 2013;57:589–96.
46. Kellogg DL, Johnson JM, Kosiba WA. Control of internal temperature threshold for active cutaneous vasodilation by dynamic exercise. J Appl Physiol. 2017;71:2476–82.
47. Itoh Y, Arai K. Use of recovery-enhanced thermography to localize cutaneous perforators. Ann Plast Surg. 1995;507–11.

48. Narushima M, Yamasoba T, Iida T, Matsumoto Y, Yamamoto T, Yoshimatsu H, et al. Pure skin perforator flaps. Plast Reconstr Surg. 2018;142:351e–60e.
49. Saint-Cyr M, Wong C, Schaverien M, Mojallal A, Rohrich RJ. The perforasome theory: vascular anatomy and clinical implications. Plast Reconstr Surg. 2009;124:1529–44.
50. Taylor GI, Corlett RJ, Dhar SC, Ashton MW. The anatomical (angiosome) and clinical territories of cutaneous perforating arteries: development of the concept and designing safe flaps. Plast Reconstr Surg. 2011;127:1447–59.
51. Venus M, Waterman J, McNab I. Basic physiology of the skin. Surgery. 2011;29:471–4.
52. Braverman IM. The cutaneous microcirculation. J Investig Dermatol Symp Proc. 2000;5:3–9.
53. Camargo CP, Gemperli R. Endothelium and cardiovascular diseases. Vascular biology and clinical syndromes. Chapter 47-Endothelial function in skin microcirculation. 2018, pp 673–679. https://doi.org/10.1016/B978-0-12-812348-5.00047-7.
54. Liu WM, Maivelett J, Kato GJ, Taylor VIJG, Yang WC, Liu YC, et al. Reconstruction of thermographic signals to map perforator vessels in humans. Quant Infrared Thermogr J. 2012;9:123–33.
55. Fry AC, Kraemer WJ. Resistance exercise overtraining and overreaching: neuroendocrine responses. Sports Med. 1997;23:106–29.
56. Zaproudina N, Varmavuo V, Airaksinen O, Närhi M. Reproducibility of infrared thermography measurements in healthy individuals. Physiol Meas. 2008;29:515–24.
57. Tse J, Rand C, Carroll M, Charnay A, Gordon S, Morales B, et al. Determining peripheral skin temperature: subjective versus objective measurements. Acta Paediatr Int J Paediatr. 2016;105:e126–31.
58. Fernández-Cuevas I, Marins JC, Carmona PG, García-Concepción MA, Lastras JA, Quintana MS. Reliability and reproducibility of skin temperature of overweight subjects by an infrared thermography software designed for human beings. Thermol Int. 2012;22:130–7.
59. Ring FJ, Ammer K, Wiecek B, Plassmann P, Jones CD, Jung A, et al. Quality assurance for thermal imaging systems in medicine. Thermol Int. 2007;17:103–6.
60. Micro-Epsilon Messtechnik. Mehr Präzision. Grundlagen der berührungslosen Temperaturmessung. 2017;4–5.
61. Tattersall GJ. Infrared thermography: a non-invasive window into thermal physiology. Comp Biochem Physiol Part A Mol Integr Physiol. 2016;202:78–98.
62. Bach AJE, Stewart IB, Disher AE, Costello JT. A comparison between conductive and infrared devices for measuring mean skin temperature at rest, during exercise in the heat, and recovery. PLoS One. 2015;10:1–13.
63. Shimazaki Y, Yoshida A, Yamamoto T. Thermal responses and perceptions under distinct ambient temperature and wind conditions. J Therm Biol. 2015;49–50:1–8.
64. Carlos J, Marins B, Formenti D, Magno C, Costa A, De Andrade A, et al. Infrared physics and technology circadian and gender differences in skin temperature in militaries by thermography. 2015;71:322–8.
65. Neves EB, Moreira TR, Lemos RJ, Vilaça-Alves J, Rosa C, Reis VM. The influence of subcutaneous fat in the skin temperature variation rate during exercise. Rev Bras Eng Biomed. 2015;31:307–12.
66. Neves EB, Salamunes ACC, de Oliveira RM, Stadnik AMW. Effect of body fat and gender on body temperature distribution. J Therm Biol. 2017;70:1–8.
67. Chudecka M, Lubkowska A. Thermal maps of young women and men. Infrared Phys Technol. 2015;69:81–7.
68. Smith CJ, Havenith G. Body mapping of sweating patterns in male athletes in mild exercise-induced hyperthermia. Eur J Appl Physiol. 2011;111:1391–404.
69. Taylor NAS, Tipton MJ, Kenny GP. Considerations for the measurement of core, skin and mean body temperatures. J Therm Biol. 2014;46:72–101.
70. Neves EB. The effect of body fat percentage and body fat distribution on skin surface temperature with infrared thermography. J Therm Biol. 2017;66:1–9.
71. Moreira DG, Costello JT, Brito CJ, Adamczyk JG, Ammer K, Bach AJE, et al. Thermographic imaging in sports and exercise medicine: a Delphi study and consensus statement on the measurement of human skin temperature. J Therm Biol. 2017;69:155–62.
72. Maniar N, Bach AJE, Stewart IB, Costello JT. The effect of using different regions of interest on local and mean skin temperature. J Therm Biol. 2015;49–50:33–8.
73. Fournet D, Redortier B, Havenith G. Institutional Repository A method for whole-body skin temperature mapping in humans. Thermol Int. 2012;22:157–9.
74. Duarte A, Carrão L, Espanha M, Viana T, Freitas D, Bártolo P, et al. Segmentation algorithms for thermal images. Proc Technol. 2014;16:1560–9.
75. Formenti D, Ludwig N, Rossi A, Trecroci A, Alberti G, Gargano M, et al. Skin temperature evaluation by infrared thermography: comparison of two image analysis methods during the non-steady state induced by physical exercise. Infrared Phys Technol. 2017;81:32–40.
76. Barcelos EZ, Caminhas WM, Ribeiro E, Pimenta EM, Palhares RM. A combined method for segmentation and registration for an advanced and progressive evaluation of thermal images. Sensors (Switzerland). 2014;14:21950–67.
77. Unger M, Markfort M, Halama D, Chalopin C. Automatic detection of perforator vessels using infrared thermography in reconstructive surgery. Int J Comput Assist Radiol Surg. 2019;14(3):501–7. https://doi.org/10.1007/s11548-018-1892-6.
78. Liu G, Jia W, Sun V, Choi B, Chen Z. High-resolution imaging of microvasculature in human skin in-vivo with optical coherence tomography. Opt Express. 2012;20:7694.
79. Cheng VS, Bai J, Chen Y. A high-resolution three-dimensional far-infrared thermal and true-color imaging system for medical applications. Med Eng Phys. 2009;31:1173–81.
80. Deng ZS, Liu J. Mathematical modeling of temperature mapping over skin surface and its implementation in thermal disease diagnostics. Comput Biol Med. 2004;34:495–521.
81. Cifuentes IJ, Dagnino BL, Salisbury MC, Perez ME, Ortega C, Maldonado D. Augmented reality and dynamic infrared thermography for perforator mapping in the anterolateral thigh. Arch Plast Surg. 2018;45:284–8.
82. Rathmann P, Chalopin C, Halama D, Giri P, Meixensberger J, Lindner D. Dynamic infrared thermography (DIRT) for assessment of skin blood perfusion in cranioplasty: a proof of concept for qualitative comparison with the standard indocyanine green video angiography (ICGA). Int J Comput Assist Radiol Surg. 2018;13:479–90.
83. Zhang H, Casaseca-de-la-Higuera P, Luo C, Wang Q, Kitchin M, Parmley A, et al. Systematic infrared image quality improvement using deep learning based techniques. 2016;10008:100080P.